Photoluminescence and thermoluminescence properties of $Ca_2PO_4Cl:Eu^{2+}$

1990 J. Phys.: Condens. Matter 2 3619

(http://iopscience.iop.org/0953-8984/2/15/017)

J. Phys.: Condens. Matter 2 (1990) 3169–3628. Printed in the UK

Photoluminescence and thermoluminescence properties of $Ca_2PO_4Cl:Eu^{2+}$

A Meijerink and G Blasse
Physics Laboratory, University of Utrecht, 3508 TA Utrecht, The Netherlands

Received 12 October 1989, in final form 28 November 1989

Abstract. In Ca_2PO_4Cl the Eu^{2+} ion occupies two different crystallographic sites. The main difference between the sites is their size. The vibronic coupling strength of the $4f^7 \rightarrow 4f^65d$ transition on Eu^{2+} is very sensitive to this difference in size resulting in Huang–Rhys factors of $S = 3$ and $S = 9$ for the two sites.

The observation of vibronic structure in combination with ^7F_J splitting in the excitation spectrum of the Eu^{2+} emission makes an accurate determination of the splitting of the $4f^6$ configuration in the $4f^65d$ excited state possible. This splitting is smaller than the free ion values for Eu^{3+}, which is probably due to a reduction of the spin–orbit coupling parameter and/or to crystal-field splitting of the ^7F_J terms.

Upon irradiation with low energy x-rays $Ca_2PO_4Cl:Eu^{2+}$ acts as a storage phosphor. Analysis of the thermoluminescence suggests a centre-to-centre recombination mechanism.

1. Introduction

In the spectroscopy involving rare earth ions, that with Eu^{2+} takes a special place. Depending on the host lattice, sharp line emission spectra due to transitions within the $4f^7$ configuration or broad band emission spectra due to $4f^65d \rightarrow 4f^7$ transitions may be observed [1–3]. The broad band absorption and emission spectra show fine structure in many cases. The fine structure may arise from splitting of the $4f^6$ core in the $4f^65d$ excited state, coupling with vibrations or Fano anti-resonance [3, 4]. Much research has been done in the past to explain the diverse luminescence behaviour of Eu^{2+} in different host lattices [5–9].

In this paper the luminescence properties of Eu^{2+} in Ca_2PO_4Cl are reported and discussed. Ca_2PO_4Cl has the spodiosite structure [10]. In this structure two different crystallographic sites are available for the divalent cation, one with site symmetry C_2 and another with site symmetry C_s. On both sites the cation is coordinated by six oxygen ions and two chlorine ions. The difference between the two sites is their size. For the larger C_s site the average Ca–O distance is 2.50 Å and the average Ca–Cl distance is 2.89 Å. For the smaller C_2 site these distances are 2.46 Å and 2.81 Å, respectively.

The luminescence properties of $Ca_2PO_4Cl:Eu^{2+}$ at 298 K have been reported by Palilla and O'Reilly [11], who found one emission band. Our measurements at low temperatures and low europium concentrations show that the Eu^{2+} ions on the two crystallographic sites have different luminescence properties. The difference in size of the two sites is reflected in a large difference between the Stokes shifts of the Eu^{2+}

0953-8984/90/153619 + 10 $03.50

emission. The excitation and emission spectra of the Eu^{2+} luminescence with the small Stokes shift show vibrational structure. The observation of vibrational structure and structure due to the splitting of the $4f^6$ configuration in the $4f^6(^7F_J)5d$ excited state makes an accurate determination of the splitting of the ^7F_J levels possible.

In the last part of this paper the thermoluminescence properties of $Ca_2PO_4Cl:Eu^{2+}$ after x-ray irradiation are discussed. It has recently been shown that halide-containing oxide-type lattices activated with divalent Eu provide efficient storage phosphors for x-ray imaging [12, 13]. Although the constituent elements in Ca_2PO_4Cl are too light to be used in medical x-ray imaging, $Ca_2PO_4Cl:Eu^{2+}$ is a storage phosphor after irradiation with x-rays. The thermoluminescence of the x-ray irradiated phosphor is analysed. The results suggest a centre-to-centre recombination mechanism, in agreement with previous results on related storage phosphors [14–16].

2. Experimental details

Powder samples of $Ca_2PO_4Cl:Eu^{2+}$ were prepared by firing an intimate mixture of $CaCl_2 \cdot 2H_2O$ (Merck, pa), $Ca(H_2PO_4)_2 \cdot H_2O$ (Baker, analysed), $CaCO_3$ (Merck, suprapur) and Eu_2O_3 (Highways, 99.99%) for 5 h at 800 °C in a reducing atmosphere (N_2/H_2). The samples were checked by x-ray powder diffraction using a Philips diffractometer (Cu Kα radiation). Photoluminescence spectra were recorded using a Perkin–Elmer MPF 44B spectrofluorometer equipped with an Oxford CF204 liquid-helium-flow cryostat. Thermoluminescence measurements were performed on x-ray (Cu Kα) irradiated samples using the same spectrofluorometer equipped with a home-made high temperature cell. Linear heating was obtained by using a programmable WEST 2050 temperature controller.

3. Results

The compound investigated, $Ca_2PO_4Cl:Eu^{2+}$, is an efficient luminescent material. The emission spectra of $Ca_{2-x}Eu_xPO_4Cl$ at 4.2 K are shown in figure 1 for $x = 0.0004$ and $x = 0.01$. For a relatively high europium concentration, e.g. $x = 0.01$, a strong emission band is observed with vibrational structure, and a weak shoulder on the shorter wavelength side. With decreasing x the relative intensity of the shoulder increases. This will be discussed below. The observation of a shoulder in the emission spectra indicates the presence of two emission bands. The vibrational structure observed for the longer wavelength emission band shows a zero-phonon line at 446.2 nm, indicated by 0 in figure 1, and phonon replicas, indicated by 1, 2 and 3 in figure 1. The positions of the phonon replicas are tabulated in table 1. The average spacing between the phonon replicas is around 110 cm^{-1}.

The excitation spectra for the longer wavelength emission ($\lambda = 460$ nm) and the shorter wavelength emission ($\lambda = 430$ nm) are shown in figure 2. The spectra are different for the two emission wavelengths. The excitation spectrum for the longer wavelength emission shows vibrational structure and is at lower energy than the excitation spectrum for the shorter wavelength emission. This shows that the longer wavelength emission band with vibrational structure and the emission band on the shorter wavelength side are due to Eu^{2+} ions on two different crystallographic sites. The sites will be

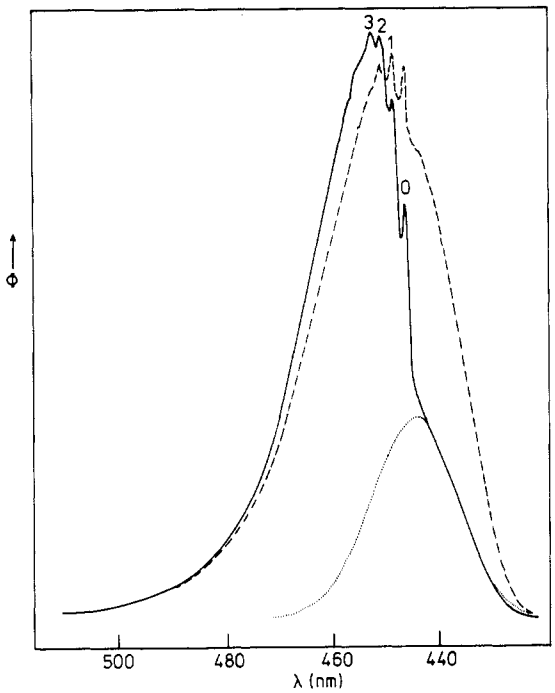

Figure 1. Emission spectra of $Ca_{1.9996}Eu_{0.0004}PO_4Cl$ (- - - -) and $Ca_{1.99}Eu_{0.01}PO_4Cl$ (——) at 4.2 K (λ_{exc} = 330 nm). The dotted curve is explained in the text. Φ gives the radiant power per constant wavelength interval in arbitrary units.

Table 1. Positions of the zero-phonon line and phonon replicas for the Eu(2) emission band in $Ca_{1.99}Eu_{0.01}PO_4Cl$ at 4.2 K.

n	λ (nm)	ΔE (cm^{-1})
0	446.2	—
1	448.5	114
2	450.8	114
3	452.9	103

referred to as Eu(1) and Eu(2), where Eu(1) corresponds to the site for which the Eu^{2+} emission is at the highest energy.

The two emission bands overlap strongly. To determine the positions of the maxima of the emission bands, the shorter wavelength emission band from Eu(1), present as a shoulder in the emission spectra, was fitted to a Gaussian-shaped band. This is possible since the longer wavelength emission band from Eu(2) will have zero intensity at 4.2 K for wavelengths shorter than that of the zero-phonon line at 446.2 nm. Therefore the observed emission intensity between 420 and about 444 nm is due to emission from Eu(1). After conversion to an energy scale the emission spectrum for $x = 0.0004$ at 4.2 K was fitted to a Gaussian between 420 and 444 nm. A good fit was obtained for a position of the maximum at 22 490 cm^{-1} (445 nm) and a width of 590 cm^{-1}. The result of this fit for the Eu(1) emission band was used to determine the position of the maximum of the longer wavelength emission band from Eu(2). The Eu(1) emission band, shown by the dotted curve in figure 1, was subtracted from the emission spectrum for $x = 0.01$ at 4.2 K.

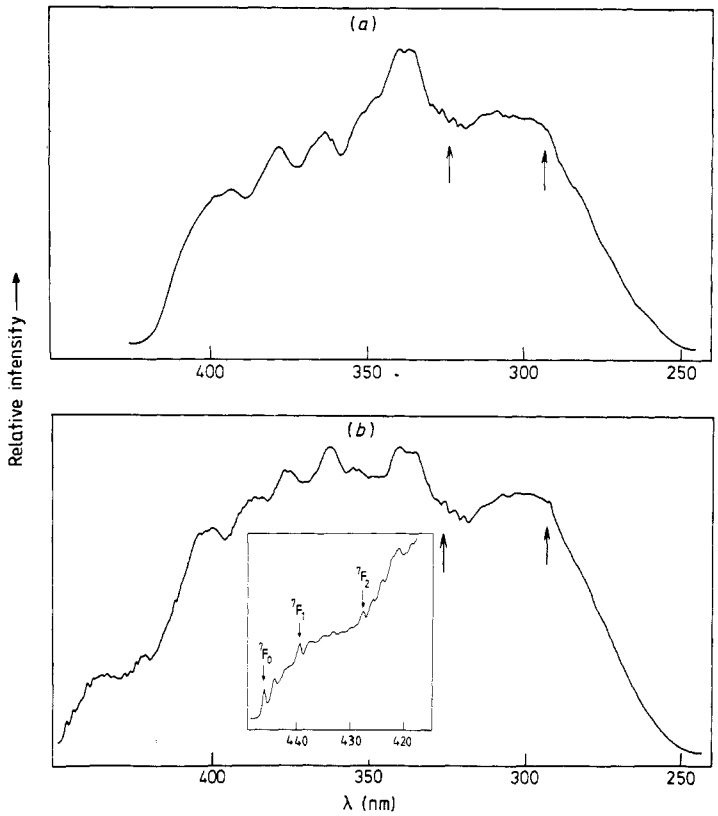

Figure 2. Excitation spectra of $Ca_{1.9996}Eu_{0.0004}PO_4Cl$ at 4.2 K for (*a*) λ_{em} = 430 nm and (*b*) λ_{em} = 460 nm. Inset: enlarged part of (*b*) showing the zero-phonon lines and phonon replicas for the $4f^7 \rightarrow 4f^6(^7F_{0,1,2})5d$ transitions in more detail. The arrows indicate Fano anti-resonance.

After subtraction the position of the maximum for the Eu(2) emission band is located at about 454 nm.

The relative intensities of the two emission bands for $x = 0.0004$ after 330 nm excitation at 4.2 K are 0.47 and 0.53 for the Eu(1) and the Eu(2) emission bands, respectively. The nearly equal intensities indicate that there is no preference of Eu^{2+} for one of the two crystallographic sites, which are present in equal amounts. The relative intensity of the zero-phonon line of the Eu(2) emission band is about 3% of the total Eu(2) emission intensity.

The excitation spectra of emission bands both show the characteristic structure of the splitting of the $4f^6$ configuration into seven $4f^6(^7F_J)5d$ bands. The excitation spectrum of the Eu(2) emission band shows, just like the emission band, vibrational structure. A zero-phonon line and phonon replicas at spacings of around 100 cm^{-1} are observed for the $4f^6(^7F_0)5d$, $4f^6(^7F_1)5d$, $4f^6(^7F_2)5d$ and $4f^6(^7F_3)5d$ excitation bands. The zero-phonon lines are located at 446.2 nm, 439.3 nm, 427.6 nm and 412.2 nm, respectively. The $^7F_0$, $^7F_1$ and $^7F_2$ zero-phonon lines are indicated by an arrow in the inset of figure 2.

Around 320 nm and 295 nm dips are observed in the excitation spectrum. These dips, indicated by arrows in figure 2, are ascribed to Fano anti-resonance due to interaction between the $4f^7(^6I_J, {}^6D_J)$ excited states and the $4f^65d$ excited states [4].

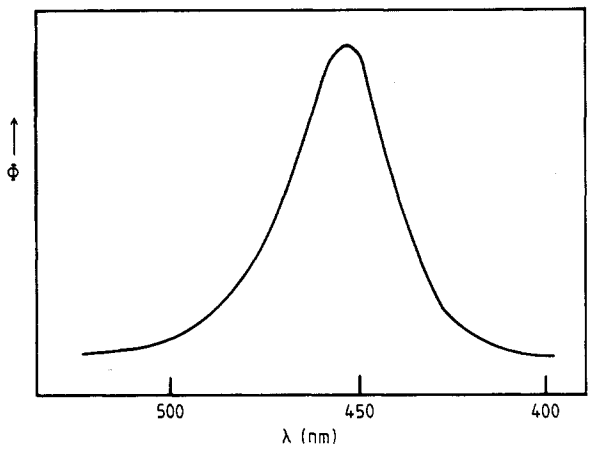

Figure 3. Emission spectrum for thermally stimulated emission at 300 K (afterglow) for x-ray (Cu Kα) irradiated $Ca_{1.99}Eu_{0.01}PO_4Cl$. Φ gives the radiant power per constant wavelength interval in arbitrary units.

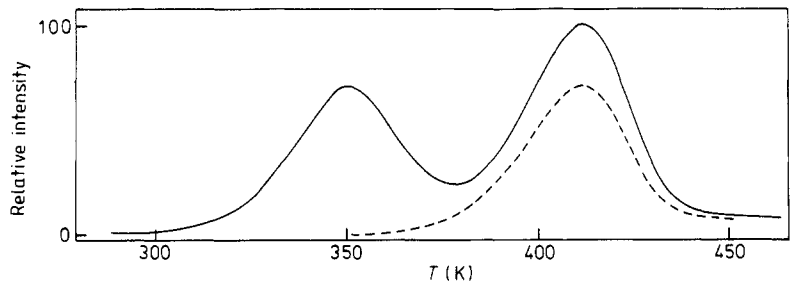

Figure 4. Thermoluminescence of $Ca_{1.99}Eu_{0.01}PO_4Cl$ for 450 nm emission after x-ray (Cu Kα) irradiation for 60 s. The heating rate β was 0.17 K s^{-1}.

After x-ray irradiation the $Ca_2PO_4Cl:Eu^{2+}$ samples show a blue afterglow. The emission spectrum of this afterglow, shown in figure 3, is a broad band with a maximum at 452 nm. This emission spectrum is identical to the Eu^{2+} emission spectrum under UV excitation at room temperature. This indicates that the thermally stimulated emission in $Ca_2PO_4Cl:Eu^{2+}$ is Eu^{2+} emission.

The glow curve for the Eu^{2+} emission at 450 nm of x-ray irradiated $Ca_{1.99}Eu_{0.01}PO_4Cl$ is shown in figure 4. The glow curve shows two peaks, one at 350 K and another at 412 K, and some weak peaks at higher temperatures. Glow curves obtained for several irradiation times between 5 and 300 s showed a linear response of the phosphor in this regime and no change of the peak positions (T_m) as a function of irradiation time.

The thermal trap depths E of the 350 K peak and the thermally cleaned 412 K peak (broken curve in figure 4) were determined using the initial rise method [17] and the peak shape method with τ (width at half height on the low temperature side), δ (width at half height on the high temperature side) and ω (full width at half height) [18]. The results, tabulated in table 1, show that the values obtained with the two methods are in good agreement. The trap depth for the 350 K peak is 6.7×10^3 cm^{-1} (0.83 eV) and for the 412 K peak 9.1×10^3 cm^{-1} (1.13 eV). Using these values the frequency factors, s, have been determined using [18]

$$s = \beta(E/kT_m^2)\exp(E/kT_m) \tag{1}$$

where β is the heating rate (0.17 K s^{-1}) and the other symbols have their usual meaning.

Table 2. Trap parameters for the two peaks in the thermoluminescence spectrum of $Ca_{1.99}Eu_{0.01}PO_4Cl$. (See also text).

T_m (K)	τ (K)	δ (K)	ω (K)	E_1 (10^3 cm^{-1})[a]	E_2 (10^3 cm^{-1})[b]	s (10^{10} s^{-1})	μ
350	16	—	—	6.6	6.8	1	—
412	18	13	31	9.2	9.0	60	0.42

[a] Thermal trap depth determined using the initial rise method.
[b] Thermal trap depth determined using the peak shape method. For the 412 K peak the average value of the trap depths obtained from τ, δ and ω is tabulated.

The geometry factor μ_g ($= \delta/\omega$) could only be determined for the thermally cleaned 412 K peak and yielded a value of 0.42. The overlap with the 412 K peak on the high temperature side of the 350 K peak makes the determination of δ, ω and μ_g impossible for the 350 K peak.

4. Discussion

4.1. Photoluminescence

The results show a clear difference between the luminescence properties of the Eu^{2+} ions on the two crystallographic sites available for Eu^{2+} in the spodiosite structure. The longer wavelength emission (from Eu(2)) is only 740 cm^{-1} Stokes shifted with respect to the $4f^6(^7F_0)5d$ excitation band, while the Stokes shift for the shorter wavelength emission amounts to 1900 cm^{-1}. The small Stokes shift for the Eu(2) emission explains the observation of vibrational structure in the excitation and emission spectra. The vibrational structure shows that the wavenumber of the vibrations with which the $4f^65d \rightarrow 4f^7$ transition has the strongest coupling, ν_{vib}, amounts to some 110 cm^{-1}. This low energy vibration is probably an Eu–O local mode. Coupling of the $4f^7 \rightarrow 4f^65d$ transition with the low energy Eu–O vibration has been observed by us before in $SrB_4O_7:Eu^{2+}$ [19] and $Ba_2B_5O_9Br:Eu^{2+}$ [20].

The Huang–Rhys factor S for the Eu(2) luminescence, determined from the Stokes shift, which equals $(2S + 1)\nu_{vib}$, is 3. This is in good agreement with the Huang–Rhys factor calculated from the relative intensity of the zero-phonon line of 0.03 which gives a Huang–Rhys factor of 3.5 [21]. For the Eu(1) luminescence the Huang–Rhys factor can be estimated from the Stokes shift of 1900 cm^{-1} to be about 9, assuming ν_{vib} to be around 100 cm^{-1}. This large difference between the Huang–Rhys factors is caused by an average difference in the distances between the Eu^{2+} ion and the coordinating anions of about 0.05 Å. This illustrates how sensitive the coupling of the $4f^7 \rightarrow 4f^65d$ transition and the lattice vibrations is to changes in the first coordination sphere.

The assignment of Eu(1) and Eu(2) to the two crystallographic sites is possible on the basis of the difference in Stokes shift. The dependence of the Stokes shift of the $4f^65d \rightarrow 4f^7$ emission of Eu^{2+} on the size of the site occupied by Eu^{2+} has been studied by measuring the quenching temperatures [22, 23] and recently also by directly measuring the Stokes shifts [20] for the Eu^{2+} emission in an isomorphous series of alkaline earth compounds. These measurements show that the Stokes shift of the Eu^{2+} emission decreases with increasing size of the site occupied by Eu^{2+}. The explanation for this

behaviour is based on a configurational coordinate diagram with $\Delta r < 0$ [24]. On the basis of these observations, the Eu(1) luminescence showing the larger Stokes shift can be assigned to the smaller C_2 site, and the Eu(2) luminescence can be assigned to Eu^{2+} on the larger C_s site.

The observation of vibrational structure in the excitation spectrum of the Eu(2) emission, in combination with the splitting of the $4f^6$ configuration in the $4f^65d$ excited state, allows an accurate determination of the splitting of the $4f^6(^7F_J)$ levels. In earlier observations, the band structure due to splitting of the $4f^6$ configuration in the $4f^65d$ excited state of Eu^{2+} was fitted to the theoretical splitting of the $4f^6$ core, for which the free ion values for Eu^{3+} were used [3, 20]. The observation of zero-phonon lines for the $^7F_0$, $^7F_1$, $^7F_2$ and $^7F_3$ excitation bands makes an accurate determination of the splitting of the ^7F_J levels in the $4f^65d$ excited state of Eu^{2+} in Ca_2PO_4Cl possible. The values obtained for the positions of the $^7F_1$, $^7F_2$ and $^7F_3$ levels with respect to the $^7F_0$ level are 347 cm^{-1}, 970 cm^{-1} and 1847 cm^{-1}, respectively. These values are smaller than the theoretical values for the spin–orbit splitting of the $4f^6$ core in Eu^{3+}; 373 cm^{-1}, 1031 cm^{-1} and 1883 cm^{-1} [25]; and smaller than the splitting usually observed for Eu^{3+} [26, 27]. This difference may be due to a reduction of the spin–orbit splitting of the $4f^6$ core of Eu^{2+} compared to that for Eu^{3+}, or to the crystal-field splitting of the $4f^6(^7F_J)$ terms in the $4f^65d$ excited state.

The spin–orbit interaction within the $4f^6$ core can be affected by exchange coupling to 5d [28]. Although this effect is expected to be small, it may cause a deviation of the observed splitting from the Eu^{3+} free ion values. Also the spin–orbit interaction parameter in the case of Eu^{2+} may be smaller than for Eu^{3+} due to the presence of the 5d electron, which induces a shift of the ligands towards the central Eu^{2+} ion. This effect is responsible for Δr being less than zero in the configurational coordinate diagram, mentioned above. It has been shown that a smaller distance between the rare earth ion and the ligands gives a reduction of the spin–orbit interaction parameter. This has been explained using a nephelauxetic effect model [29]. An alternative explanation for this effect is based on a dielectric screening model [30, 31]. These arguments can explain in a qualitative way the smaller values observed for the splitting of the $4f^6$ core in Eu^{2+} compared with that in Eu^{3+}.

In a different explanation the ^7F_J terms in the $4f^6(^7F_J)5d$ excited state are considered to be split by the crystal field. The crystal-field splitting for the $4f^6(^7F_J)$ levels in eight-fold coordination is $\simeq$100–150 cm^{-1} [32]. This splitting will shift the lowest Stark level $\simeq$50–75 cm^{-1} below the barycentre of the $^7F_1$, $^7F_2$ and $^7F_3$ levels. This can explain the shift of the zero-phonon lines of the lowest Stark levels of the $^7F_1$, $^7F_2$ and $^7F_3$ levels to lower energies with respect to the $^7F_0$ level, which is not split by the crystal field. The order of magnitude of the observed shifts, 25–50 cm^{-1}, is in agreement with the shifts expected for a crystal-field splitting of the ^7F_J levels in eight-fold coordination observed for Eu^{3+}. The crystal-field splitting of the ^7F_J levels can be somewhat smaller in the $4f^65d$ state of Eu^{2+} due to additional screening by the 5d electron.

The observation of different patterns for the phonon side band structure of the different $4f^6(^7F_J)5d$ zero-phonon lines supports the second explanation. In the absence of additional splitting a repetition of the phonon side band structure observed for the $^7F_0$ level is expected on the high energy side of the $^7F_1$, $^7F_2$ and $^7F_3$ zero-phonon lines. The presence of transitions to higher energetic Stark levels can explain the observation of different structures on the high energy side of the four zero-phonon lines.

The observed decrease of the relative amount of the Eu(1) emission intensity with increasing europium concentration is due to energy transfer from Eu(1) to Eu(2). The

large spectral overlap ($0.2\,eV^{-1}$) between the Eu(1) emission band and the Eu(2) excitation band makes the energy transfer efficient. The critical distance for energy transfer has been calculated from the relative intensity of the Eu(1) emission at different europium concentrations [20] and with the Förster–Dexter theory for energy transfer via electric dipole–dipole interaction [33, 34]. With the first method critical distances for energy transfer between 16 Å and 20 Å were obtained for europium concentrations between $x = 0.01$ and $x = 0.0004$, where x is defined in $Ca_{2-x}Eu_xPO_4Cl$. The Förster–Dexter theory gives a value of 20 Å for the critical distance for energy transfer, using a spectral overlap of $0.2\,eV^{-1}$, determined from the spectra, and an oscillator strength of 0.01 for the $4f^7 \rightarrow 4f^6(^7F_J)5d$ absorption band [35]. The good agreement between the two values shows the applicability of the Förster–Dexter theory for dipole–dipole interaction to the efficient energy transfer between inequivalent Eu^{2+} ions.

4.2. Thermally stimulated emission

Upon x-ray irradiation, storage of energy occurs in Eu^{2+}-doped Ca_2PO_4Cl. Studies on related Eu^{2+}-doped halide-containing storage phosphors [12–16] showed that the storage properties are due to the trapping of free charge carriers created by x-ray irradiation. The holes are trapped on Eu^{2+} and the electrons in halide vacancies. Upon heating, recombination of the trapped charge carriers is stimulated resulting in Eu^{2+} emission.

The geometry factor of 0.42 for the 412 K peak in the glow curve indicates the presence of first-order kinetics for this peak [36]. The asymmetrical shape of the 350 K peak suggests a first-order kinetics mechanism for this peak as well. The presence of first-order kinetics is confirmed by the measurement of the thermoluminescence spectra as a function of the irradiation dose in the range of a linear response. No shift of the peak position was observed upon changing the irradiation dose by nearly two orders of magnitude. In the case of higher order kinetics a shift of T_m to higher temperatures is expected to occur when the irradiation dose is decreased [37]. The absence of this shift confirms that the recombination mechanism is of first order for both peaks.

The observation of first-order kinetics in the thermoluminescence spectra of similar Eu^{2+}-doped storage phosphors has been reported before by us [14, 38]. The first-order kinetics in combination with low-frequency factors was explained by a centre-to-centre recombination model. For the case of centre-to-centre recombination it has been shown by Chen and Kirsch [39] that first-order kinetics is observed. The frequency factor equals $s\gamma/(s + \gamma)$ in this case, where s is the usual frequency factor ($\sim 10^{12}$–$10^{13}\,s^{-1}$) and γ is the recombination rate. This explains the observation of small frequency factors in the case of centre-to-centre recombination.

The present results on the thermoluminescence properties of $Ca_2PO_4Cl:Eu^{2+}$ suggest that the thermally stimulated luminescence is due to centre-to-centre recombination for the two major peaks in the TL spectrum, since for both peaks first-order kinetics in combination with relatively low frequency factors are observed. Centre-to-centre recombination in this type of x-ray storage phosphors has been suggested before [14–16]. The observation of centre-to-centre recombination indicates that the electron trapped in the F centre is close to the hole trapped on Eu^{3+}. The appearance of two peaks in the TL spectrum is ascribed to the presence of two different types of $(Eu._{Ca}\,V^{\times}_{Cl})$ clusters after x-ray irradiation with different thermal trap depths. In view of the two crystallographic positions available, it is not surprising to find two centres. No further information on the nature of the two different clusters can be obtained from

the thermoluminescence spectra. The weak peaks in the high temperature region of the TL spectrum ($T > 430$ K) were not analysed. They may correspond to a small fraction of electrons trapped in oxygen vacancies.

5. Conclusions

The two sites for Eu^{2+} in Ca_2PO_4Cl give rise to different luminescence properties. The average difference in the Eu anion distance of about 0.05 Å has a large influence on the Huang–Rhys factors, which are 3 and 9 for the luminescence of the Eu^{2+} ion on the two sites. This observation illustrates the sensitivity of the vibronic coupling strength of the $4f^7 \rightarrow 4f^65d$ transition on Eu^{2+} to changes in the first coordination sphere.

The excitation spectrum of the Eu^{2+} emission with the small Stokes shift shows vibrational structure in combination with structure due to the splitting of the $4f^6$ configuration in the $4f^65d$ excited state. This makes an accurate determination of the splitting of the $4f^6(^7F_J)$ levels from the positions of the zero-phonon lines possible. The observed splitting is smaller than the free ion splitting for Eu^{3+}. This is probably due to a reduction of the spin–orbit coupling parameter and/or to crystal-field splitting of the $4f^6(^7F_J)5d$ levels.

Upon x-ray excitation, energy is stored in $Ca_2PO_4Cl:Eu^{2+}$. Analysis of the glow curves suggests a centre-to-centre recombination mechanism in this phosphor.

References

[1] Blasse G 1973 *Phys. Status Solidi* b **55** K131
[2] Hoffmann M V 1971 *J. Electrochem. Soc.* **118** 933
[3] Ryan F M, Lehman W, Feldman D W and Murphy J 1974 *J. Electrochem. Soc.* **121** 1475
[4] Meijerink A and Blasse G 1989 *Phys. Rev.* B **40** 7288
[5] Alcalá R, Sardar D K and Sibley W A 1982 *J. Lumin.* **27** 273
[6] Bryukvin V V, Voropai E S, Nizhnikov V V, Parfianovich I A and Penzina E E 1986 *Opt. Spectrosk.* **60** 473
[7] Hewes R A and Hoffmann M V 1971 *J. Lumin.* **3** 261
[8] Weakliem H A 1972 *Phys. Rev.* B **6** 2743
[9] Yamashita N, Yamamoto I, Ninagawa K, Wada T, Yamashita Y and Nakao Y 1985 *Japan. J. Appl. Phys.* **24** 1174
[10] Banks E, Greenblatt M and Post B 1970 *Inorg. Chem.* **9** 2259
[11] Palilla F C, O'Reilly B E and Abbruscato V J 1970 *J. Electrochem. Soc.* **117** 87
[12] Sonoda M, Takano M, Miyahara J and Kato H 1983 *Radiology* **148** 833
[13] Meijerink A, Blasse G and Struye L 1989 *Mater. Chem. Phys.* **21** 26
[14] Meijerink A and Blasse G 1988 *Electrochem. Soc. Fall Meeting (Chicago, 1988); Proc. Symp. on Luminescence and Technology* vol 88–24, p 279
[15] van Seggern H, Voigt T, Knüpfer W and Lange G 1988 *J. Appl. Phys.* **64** 1405
[16] van Seggern H, Meijerink A, Voigt T and Winnacker A 1989 *J. Appl. Phys.* **66** 4418
[17] Garlick G F J and Gibson A F 1948 *Proc. Phys. Soc.* **60** 574
[18] Chen R 1969 *J. Electrochem. Soc.* **116** 1254
[19] Meijerink A, Nuyten J and Blasse G 1989 *J. Lumin.* **44** 19
[20] Meijerink A and Blasse G 1989 *J. Lumin.* **43** 283
[21] Imbush G F 1978 *Luminescence Spectroscopy* ed. M D Lumb (London: Academic) ch 1
[22] Blasse G, Wanmaker W L, ter Vrugt J W and Bril A 1968 *Philips Res. Rep.* **23** 189
[23] Blasse G and Bril A 1968 *Philips Res. Rep.* **23** 201
[24] Blasse G and Bril A 1970 *Philips Tech. Rev.* **10** 314
[25] Chang N C and Gruber J B 1964 *J. Chem. Phys.* **41** 3227
[26] Richardson F S, Reid M F, Dallara J J and Smith R D 1985 *J. Chem. Phys.* **83** 3813

[27] Carnall W T, Fields P R and Rajnak K 1968 *J. Chem. Phys.* **49** 4450
[28] Weakliem H A 1972 *Phys. Rev.* B **49** 2743
[29] Jørgensen C K and Reisfeld R 1977 *Lasers and Excited States of Rare Earths* ed M Becke, M F Lappert, J L Margrave and R W Parry (Berlin: Springer) ch 3
[30] Morrison C, Mason D R and Kikuchi C 1967 *Phys. Lett.* **24A** 607
[31] Newman D J 1973 *J. Phys. Chem. Solids* **34** 541
[32] Blasse G and Bril A 1970 *J. Lumin.* **3** 109
[33] Förster Th 1948 *Ann. Phys., Lpz.* **2** 55
[34] Dexter D L 1953 *J. Chem. Phys.* **21** 836
[35] Blasse G 1969 *Philips Res. Rep.* **24** 131
[36] Chen R 1969 *J. Electrochem. Soc.* **116** 1254
[37] McKeever S W S 1985 *Thermoluminescence of Solids* ed R W Cahn, E A Davis and I M Ward (Cambridge: Cambridge University Press) p 70
[38] Meijerink A and Blasse G 1990 *J. Phys. D: Appl. Phys.* submitted
[39] Chen R and Kirsch Y 1981 *Analysis of Thermally Stimulated Processes* (Oxford: Pergamon) p 33